

# Dynamics of wind and the dusty environments in the accreting T Tauri stars RY Tau and SU Aur

P. P. Petrov<sup>1</sup>★, K. N. Grankin<sup>1</sup>, J. F. Gameiro<sup>2,3</sup>, S. A. Artemenko<sup>1</sup>, E. V. Babina<sup>1</sup>, R. M. G. de Albuquerque<sup>2,3,4</sup>, A. A. Djupvik<sup>5</sup>, G. F. Gahm<sup>6</sup>, V. I. Shenavrin<sup>7</sup>, T. R. Irsamambetova<sup>7</sup>, M. Fernandez<sup>8</sup>, D. E. Mkrtichian<sup>9</sup>, and S. Yu. Gorda<sup>10</sup>

<sup>1</sup>Crimean Astrophysical Observatory of Russian Academy of Sciences, p/o Nauchny, 298409, Republic of Crimea

<sup>2</sup>Instituto de Astrofísica e Ciências do Espaço, Universidade do Porto, CAUP, Rua das Estrelas, PT4150-762 Porto, Portugal

<sup>3</sup>Departamento de Física e Astronomia, Faculdade de Ciências, Universidade do Porto, Rua do Campo Alegre 687, PT4169-007 Porto, Portugal

<sup>4</sup>Laboratoire Univers et Théories, Observatoire de Paris, UMR 8102 du CNRS, Université Paris Diderot, F-92190 Meudon, France

<sup>5</sup>Nordic Optical Telescope, Rambla José Ana Fernández Pérez, 7, 38711 Breña Baja, Spain

<sup>6</sup>Department of Astronomy, AlbaNova University Center, Stockholm University, Sweden

<sup>7</sup>Sternberg Astronomical Institute, M. V. Lomonosov Moscow State University, Moscow, Russia

<sup>8</sup>Institute of Astrophysics of Andalusia-CSIC, Glorieta de la Astronomía, 3, 18008 Granada, Spain

<sup>9</sup>National Astronomical Research Institute of Thailand, 260 Moo 4, T. Donkaew, A. Maerim, Chiangmai, 50180 Thailand

<sup>10</sup>Ural Federal University, 51, Lenin av., Ekaterinburg, Russia, 620000

Accepted XXX. Received YYY; in original form ZZZ

## ABSTRACT

Classical T Tauri stars with ages of less than 10 Myr possess accretion discs. Magnetohydrodynamic processes at the boundary between the disc and the stellar magnetosphere control the accretion and ejections gas flows. We carried out a long series of simultaneous spectroscopic and photometric observations of the classical T Tauri stars RY Tau and SU Aur with the aim to quantify the accretion and outflow dynamics at time scales from days to years. It is shown that dust in the disc wind is the main source of photometric variability of these stars. In RY Tau we observed a new effect: during events of enhanced outflow the circumstellar extinction gets lower. The characteristic time of changes in outflow velocity and stellar brightness indicates that the obscuring dust is near the star. The outflow activity in both stars is changing on a time scale of years. Periods of quiescence in H $\alpha$  profile variability were observed during 2015-2016 season in RY Tau and during 2016-2017 season in SU Aur. We interpret these findings in the framework of the magnetospheric accretion model, and discuss how the global stellar magnetic field may influence the long-term variations of the outflow activity.

**Key words:** Stars: variables: T Tauri, Herbig Ae/Be – Stars: winds, outflows – Line: profiles – Stars: individuals: RY Tau, SU Aur

## 1 INTRODUCTION

Young stars possess accretion discs at the beginning of their evolution. For solar mass stars the lifetimes of these discs are a few million years. Eventually the disc dissipates and the mass accretion ceases. Classical T Tauri stars (cTTS) are young low mass stars ( $M < 2\text{--}3 M_{\odot}$ ) with accretion discs. Their characteristic emission line spectrum, irregular light variability, and non-stationary outflows are consequences of the interaction of the accreting gas with the stellar magnetic field. When accretion ceases, the outflows disappear and the emission line spectra become weak. These are the weak-line

T Tauri stars (wTTS). This phase is much longer, 10-100 Myr, until the star eventually reaches the main sequence.

The current view of cTTS and their environments is based on the magnetospheric accretion model, initially designed for neutron stars (Ghosh & Lamb 1979) and later applied for cTTS (Camenzind 1990; Koenigl 1991). According to the models, the accretion disc of a cTTS is truncated by a stellar magnetic field at a distance of a few stellar radii. The magnetic field penetrates the inner part of the disc and thus the gas of the disc can flow down to the stellar surface along the field lines. A shock is formed at the base of the accretion channel. X-ray and UV radiation of the accretion shock ionize the infalling gas, thus giving rise to the characteristic emission line spectrum of a cTTS. The mass accretion rates

★ E-mail: petrov@crao.crimea.ru

in cTTS are in the range of  $10^{-10}$  to  $10^{-7} M_{\odot} \text{ yr}^{-1}$ . The inner accretion disc radii in cTTS, measured by near-infrared interferometry, are typically within 0.1-0.3 AU (Millan-Gabet et al. 2007). Observed properties and models of cTTS can be found in reviews by e.g. Petrov (2003), Bouvier et al. (2007), and Hartmann et al. (2016).

Besides the accretion flows, cTTS are also characterized by powerful outflows. Large scale ordered magnetic fields are thought to play a key role in forming these gas flows. Different types of winds have been considered, including a stellar wind flowing along the open magnetic field lines in the polar regions of the star (Cranmer 2009), and a disc wind, starting from the extended surface of the accretion disc and accelerated by the magnetic centrifuge of the rotating disc (Blandford & Payne 1982; Pudritz & Norman 1986; Matt & Pudritz 2005). Other possible types of winds originate from the inner region of the disc, at the boundary between the disc and the magnetosphere, either as a so called “X-wind” (Shu et al. 1994) or a “conical wind” (Romanova et al. 2009). The region where the magnetic flux connects the disc with the star is very unstable, where magnetospheric ejections of plasma can take place (Goodson et al. 1997; Zanni & Ferreira 2013). Magneto-hydrodynamic (MHD) simulations of the accretion and outflow processes in cTTS have been performed by several groups (see reviews by Bouvier et al. (2007), Romanova & Owocki (2015) and references therein). The gas flows can be traced by analysis of emission line profiles in spectra of cTTS. Specific profiles of Hydrogen and Helium lines were calculated for different wind models (e.g., Kurosawa et al. 2011; Grinin et al. 2012). The disc wind also contributes to the irregular light variability of cTTS. Beyond the dust sublimation radius, the disc wind is dusty, which causes circumstellar extinction of cTTS.

The processes of accretion and the accretion-driven winds are non-stationary. Dynamics of the gas flows depends of the conditions at the boundary between the disc and stellar magnetosphere. The stellar magnetosphere may be not axisymmetric, which causes rotational modulation of the observed flows. The rotational modulations in the emission lines were observed in some cTTS, e.g. in RW Aur A (Petrov 2003) and also simulated in the MHD models (e.g. Romanova et al. 2007).

Long term variations in the outflow activity may be controlled by the variable mass accretion rate and/or gradual change in the global stellar magnetic field. Variations in the magnetic fields of cTTS were reported by Donati et al. (2011, 2012).

In this paper we present results of our spectroscopic monitoring of two cTTS, SU Aur and RY Tau, during several years. Besides long-term changes in the wind activity, we were interested to know whether short-term wind dynamics is reflected in the irregular variations of the circumstellar extinction. For that reason, the spectroscopy was supported by simultaneous photometry of the stars. Preliminary results of the first two years of our monitoring of RY Tau were previously published in Babina et al. (2016).

The paper is organized as follows. In Sect. 2 we start with review of basic data for SU Aur and RY Tau and proceed with a description of our observations in Sect. 3. The results obtained are given in Sect. 4 and discussed in Sect. 5. Finally, the conclusions are listed in Sect. 6.

## 2 BASIC DATA FOR SU AUR AND RY TAU

In this Section we compare observed characteristics of RY Tau and SU Aur to outline their similarities and differences. Both stars belong to intermediate mass classical T Tauri stars. They are located in the Taurus-Auriga star forming region at a distance of about 140 pc (Elias 1978; Loينard et al. 2007). The basic parameters of the stars according to Calvet et al. (2004) are  $T_{\text{eff}} = 5945 \pm 142.5$  K for both stars and stellar luminosities  $L = 9.6 \pm 1.5 L_{\odot}$  in RY Tau and  $7.8 \pm 1.3 L_{\odot}$  in SU Aur.

The parallaxes measured by GAIA<sup>1</sup> give the following distances:  $142.4 \pm 12$  pc for SU Aur and  $176.6 \pm 27$  pc for RY Tau, i.e. the distance to RY Tau could be somewhat larger than usually assumed. However, one should take into account the most accurate measurements of parallaxes of several TTS in the Taurus complex obtained in the multi-epoch VLBA array observations (Loينard et al. 2007). They found a mean distance to the star-forming region of about 140 pc with a depth of around 20 pc. Hence, the upper limit of the distances measured by VLBA (150 pc) coincides with the lower limit of the distance to RY Tau (149.6 pc) obtained by GAIA. Therefore, we adopt a distance to RY Tau of  $150 \pm 10$  pc.

### 2.1 Light variability

Both objects have long photometric records. RY Tau has shown irregular variability within  $V = 9.5 - 11.5$ , with noticeable brightening in 1983-1984 and 1996-1997 (Herbst & Stine 1984; Herbst et al. 1994; Zajtseva et al. 1996). The most extended series of photometric observations of RY Tau from 1965 to 2000 was analysed by Zajtseva (2010). Quasi-periodic variations of brightness, probably associated with eclipses by dust cloud in the circumstellar disc were revealed. No periodicity related to rotation of the star itself was detected.

SU Aur is an irregular variable, most of time at  $V = 9.0 - 9.5$  with random drops down to  $V = 10 - 11$  (Herbst & Shevchenko 1999; DeWarf et al. 2003). Possible periods of 1.55 and 2.73 days were reported by Herbst et al. (1987), but not confirmed later (Herbst & Koret 1988). Bouvier et al. (1988, 1993) reported a possible period of 2.78 days, which is close to the rotational period derived from spectral lines variations (see below). MOST photometry (Cody et al. 2013) showed small amplitude ( $\sim 0.1$  mag) brightness oscillations with period of  $\sim 2.7$  days over 20 days of observation.

### 2.2 Emission line spectra

The emission line spectra of RY Tau and SU Aur are not as strong as in late-type cTTS, because of the luminous background of the G-type photosphere. In the optical spectrum of SU Aur only  $H\alpha$  is in emission. In RY Tau the emission spectrum includes  $H\alpha$ ,  $H\beta$ , the Na I doublet, He I 5876 Å, Ca II doublet and the NIR Ca II triplet (e.g. Hamann & Persson 1992; Alencar & Basri 2000). Forbidden emission lines

<sup>1</sup> <http://gaia.ari.uni-heidelberg.de/singlesource.html>

of [O I], [N II], [S II] and [Fe II] were observed in the spectrum of RY Tau (Cabrit et al. 1990; Akitaya et al. 2009). No forbidden lines have been reported for SU Aur.

The photospheric spectrum of a cTTS is often veiled by additional radiation from hot surface areas at the base of accretion columns. The effect is stronger in a late type cTTS where the brightness contrast of the hot area is larger. The veiling of the photospheric spectrum of RY Tau in the visual range is very low or absent (Basri et al. 1991; Hartigan et al. 1995; Petrov et al. 1999; Chou et al. 2013). No veiling in the visible photospheric spectrum of SU Aur has been reported. Excess continuous radiation is present in the far UV spectrum of both stars, larger in RY Tau than in SU Aur. The mass accretion rates, estimated from the accretion luminosities in UV, are  $6.4 - 9.1 \pm 4.9$  for RY Tau, and  $0.5 - 0.6 \pm 0.4$  for SU Aur, in units of  $10^{-8} M_{\odot} \text{ yr}^{-1}$  (Calvet et al. 2004).

Near and Far-UV spectra of TTS, including RY Tau and SU Aur, were analysed by Ardila et al. (2002); Gomez de Castro & Verdugo (2007); Gomez de Castro & Marcos-Arenal (2012). A catalogue of selected atomic and molecular line fluxes, observed in the Far IR, is presented in Alonso-Martinez et al. (2017).

### 2.3 Rotation and X-rays

Both stars are rapid rotators. In SU Aur, the  $v \sin i$  is within  $= 60 - 66 \text{ km s}^{-1}$  (Nguyen et al. 2012; Johns-Krull 1996; Petrov et al. 1996). In RY Tau, the  $v \sin i \sim 50 \text{ km s}^{-1}$  (Petrov et al. 1999). The rotation period of SU Aur is within 2.7 - 3.0 days, as determined from periodical modulations of the blue- and red-shifted absorption components in the Balmer line profiles (Giampapa et al. 1993; Johns & Basri 1995; Petrov et al. 1996) and strength of He I emission lines (Unruh et al. 2004). In RY Tau no rotation period was detected, neither from the extended photometric series or from the emission lines variations. Both RY Tau and SU Aur are X-ray sources. RY Tau is a strong, flaring X-ray source, indicating radiation from a hot plasma at  $T \sim 50 \text{ MK}$ . The flaring component is undoubtedly of magnetic origin (Skinner et al. 2016). The quiescent X-ray emission from SU Aur is dominated by a 20 - 40 MK plasma, while an extremely high temperature plasma component (at least 60 MK) was observed in a flare (Smith et al. 2005).

### 2.4 Discs and jets

Both stars possess accretion discs, as indicated by their spectral energy distribution (SED) and interferometry in the infrared (IR). The SED of RY Tau and SU Aur from SPITZER mid-IR observations (Furlan et al. 2011) represents radiation of warm layers from an inner disc within 10 AU.

A number of accretion disc models of RY Tau and SU Aur has been presented to reproduce the IR observations, e.g. Muzerolle et al. (2003), Akeson et al. (2005), Schegerer et al. (2008), Isella et al. (2010), and Guilloteau et al. (2011). The inner disc radius in different models drops within 0.3 - 0.5 AU, and inclinations of the disc axis to the line of sight appear within 55 - 75 °.

Imaging polarimetry of SU Aur has shown that the accretion disc extends out to 500 AU with an inclination of  $\sim$

50° (Jeffers et al. 2014); the disc morphology with tidal tails was reconstructed by De Leon et al. (2015). Imaging polarimetry of RY Tau (Takami et al. 2013) showed that the scattered light in the near-IR is associated with an optically thin and geometrically thick layer above the disc surface. The changes in the linear polarization across the  $H\alpha$  line in RY Tau and SU Aur are consistent with the presence of a compact source of line emission that is scattered off a rotating inner accretion disc (Vink et al. 2005).

Extended bipolar jets of RY Tau, with young dynamical ages of the inner knots, were detected in  $H\alpha$  light (St-Onge & Bastien 2008) and mapped in [O I] 6300 Å (Agra-Amboage et al. 2009). Spatially resolved C IV emission from the blue-shifted jet of RY Tau has been detected by Skinner et al. (2018).

In summary, RY Tau and SU Aur are rather similar with regard to stellar parameters, but with different accretion rates and circumstellar environments. The high inclinations of both stars implies that the line of sight intersects the disc winds. This provides an opportunity to search for dynamics of the circumstellar gas flows through variability in spectral line profiles.

### 2.5 Spectral time series

A typical characteristics of the gas flows in cTTS is their non-stability on time scales of a day and longer. In some cases, spectral monitoring can reveal modulation of a line profile with a period of the stellar rotation, which may be due to axial asymmetry of the gas flows.

Several extended time series of high-resolution spectroscopic observations have been obtained for SU Aur (Giampapa et al. 1993; Johns & Basri 1995; Petrov et al. 1996; Oliveira et al. 2000; Unruh et al. 2004). The Balmer line profiles show the largest variability in the blue-shifted and red-shifted depressions of the broad emission profiles, formed in the outflow (wind) and inflow (accretion) gas streams. Variations in the blue wing of  $H\alpha$  and  $H\beta$  revealed rotational period about 3.0 days (Giampapa et al. 1993; Johns & Basri 1995; Petrov et al. 1996). A shorter period of 2.6 to 2.8 days was found in variations of the He I D3 line (Unruh et al. 2000, 2004). Time-series involving  $\text{Pa}\beta$  spectroscopy of SU Aur over three consecutive nights showed relatively strong variability in the red wing within a radial velocity range of 100 - 420  $\text{km s}^{-1}$ , and less variability in the blue wing. A model with an inclined dipole magnetosphere reproduced the observed line variability (Kurosawa et al. 2005). Sometimes a strong depression of the blue wing of  $H\alpha$  appeared, indicating enhanced sporadic mass ejections (Petrov et al. 1996).

Time variability of the emission lines in RY Tau were studied by Zajtseva et al. (1985), Petrov (1990), Johns & Basri (1995), Smith et al. (1999), Mendigutía et al. (2011), and Chou et al. (2013). The broad emission profiles of the  $H\alpha$  line is cut by a deep blue-shifted depression. Both the blue and red peaks of the line are variable on a time scale of a few days. Balmer  $H\alpha$  line monitoring of RY Tau in 37 almost fully contiguous nights (Johns & Basri 1995) did not reveal any periodicity similar to SU Aur. Although both RY Tau and SU Aur are fast rotators with similar stellar parameters, axial rotation of RY Tau is not reflected as variability in the Balmer line profiles. Ismailov et al. (2015) reported possible

period of 23 days in variability of the Mg II 2800 Å emission line intensity in IUE spectra of RY Tau. This is close to the periods found from photometric series (Bouvier et al. 1993; Gahm et al. 1993a). This long period is certainly not related to the stellar rotation.

### 3 OBSERVATIONS

Our spectral and photometric observations were carried out during five seasons of 2013-2018. We started with observations of RY Tau at the Crimean Astrophysical Observatory (CrAO) in the 2013-2014 and 2014-2015 seasons. Then, a multi-site monitoring of RY Tau and SU Aur was arranged in 2015-2016 season. Later we proceeded with observations of RY Tau and SU Aur, mostly at CrAO. In all the seasons, photometry of our targets were performed at three telescopes, located in Crimea.

#### 3.1 Spectroscopy

The following five instruments were used to obtain series of spectral observations of RY Tau and SU Aur.

(1) 2.6-m Shajn reflector of the Crimean Astrophysical Observatory (CrAO) with echelle spectrograph. Spectral resolution  $R=27000$  with entrance slit  $2''$ .

(2) 2.5-m Nordic Optical Telescope (NOT) with ALFOSC grism spectrograph, grism set #17, registered spectral region 6330-6870 Å,  $R=10000$  with entrance slit  $0.5''$ .

(3) 2.2-m telescope at Centro Astronómico Hispano-Alemán (CAHA) with CAFE echelle spectrograph,  $R=58000$  with entrance slit  $1.2''$ .

(4) 2.4-m Thai National Telescope (TNT) at Thai National Observatory (TNO) with Medium Resolution Spectrograph (MRES),  $R=19000$  with entrance fiber  $2''$ .

(5) 1.2-m telescope of Kourovka Astronomical Observatory of the Ural Federal University (UrFU), with fiber-fed echelle spectrograph,  $R=15000$ , entrance fiber  $5''$  (Panchuk et al. 2011).

Further details on the spectrographs can be found at the corresponding web-sites of the observatories. All spectra were reduced and wavelength calibrated using standard procedures and IRAF tools. In the echelle spectra we utilized only those spectral orders which cover regions of the H $\alpha$  and Na D lines. Signal-to-noise ratio per resolution element at the continuum level in all the spectra was over 100. Total number of nights of spectral observations: 127 for RY Tau and 96 for SU Aur. Log of spectral observations is given in Table 1A and Table 2A.

#### 3.2 Photometry

Optical photometry of RY Tau and SU Aur in the Johnson BVRI photometric system was carried out with two instruments: 1.25-m telescope (AZT-11) of the Crimean Astrophysical Observatory (CrAO), and 0.6-m telescope (Zeiss-600) at the Crimean Astronomical Station (CAS) of Moscow State University. At the 1.25-m telescope, photometer with FLI PL23042 CCD camera was used for a routine differential photometry, while in cases of perfectly clear sky a

photo-counting photometer was used for absolute photometry. The standard error is about 0.02 mag in all bands. At the 0.6 m telescope, photometer with CCD cameras Apogee Aspen and PL4022 was used.

Near Infrared (NIR) photometry was carried out at the 1.25-m telescope of CAS. InSb-photometer with a standard JHKLM system was used. Technical parameters of the photometer, methods of observations and calculations of magnitudes were described in details by Shenavrin et al. (2011). Stars BS1203 and BS1791 were used as standards for RY Tau and SU Aur correspondingly. JKL magnitudes of the standards were taken from the catalogue of Johnson et al. (1966), and HM magnitudes were calculated from relations given in Koornneef (1983). The standard error of the measured magnitudes is about 0.02 in JHKL bands, and about 0.05 in M band. In addition, we used also photometric data from the American Association of Variable Star Observers (AAVSO) (Kafka 2017).

The results of the photometric observations in V-band are presented in form of light-curves in Fig. 1 and 2, where moments of spectral observations are marked with vertical bars. AAVSO data are added to the figure to make the lightcurves more dense. V-magnitudes in the dates of spectral observations are presented also in Tables A1 and A2 for RY Tau and SU Aur, respectively. In case we had no photometric observation at the date of spectral observation, the V-magnitude was taken either from AAVSO data or from linear interpolation between the nearest dates in the photometric series. The probable error of the interpolated V-mag was roughly estimated as 0.1 mag taking into account the typical gradients in the light-curves. The results of the NIR photometry for both stars is given in Tables A3 and A4, where we include also visual photometry, when available at the dates of NIR photometry. Our previous NIR photometry of RY Tau in 1981-1997 is also included in Table A3.

## 4 RESULTS

### 4.1 Photometry

We start the analysis of the observations with a revision of the basic stellar parameters of RY Tau and SU Aur. From optical photometry we estimate the interstellar extinction  $A_V$  and calculate the absolute magnitude  $M_V$ . We adopt  $T_{\text{eff}} = 5945 \pm 140$  K (Calvet et al. 2004), which corresponds to spectral type G1-G2 IV. Then, with  $T_{\text{eff}}$  and  $M_V$  we enter the PMS models by Siess et al. (2000) and get the stellar luminosity, mass, radius and age.

In Fig. 3 and 4 we plot colour-magnitude diagrams using the most extended and uniform photometric data collected at Majdanak observatory over 20 years (Grankin et al. 2007). The brightest V magnitudes ( $V_{\text{max}}$ ) in the diagrams supposedly represent the normal brightness of the star, not obscured by circumstellar matter. We use  $(V - R_j)$  colours to estimate the interstellar reddening. A star with  $T_{\text{eff}} = 5945$  K has an intrinsic colour of  $(V - R_j) = 0.52$  mag (Kenyon & Hartmann 1995). The unreddened V magnitudes, corresponding to the intrinsic  $(V - R_j)$  colour, are  $V = 8.20$  mag for SU Aur and  $V = 8.00$  mag for RY Tau, as indicated by the cross-section of the reddening lines with the dashed lines. With an error of the adopted  $T_{\text{eff}}$  about 142 K and

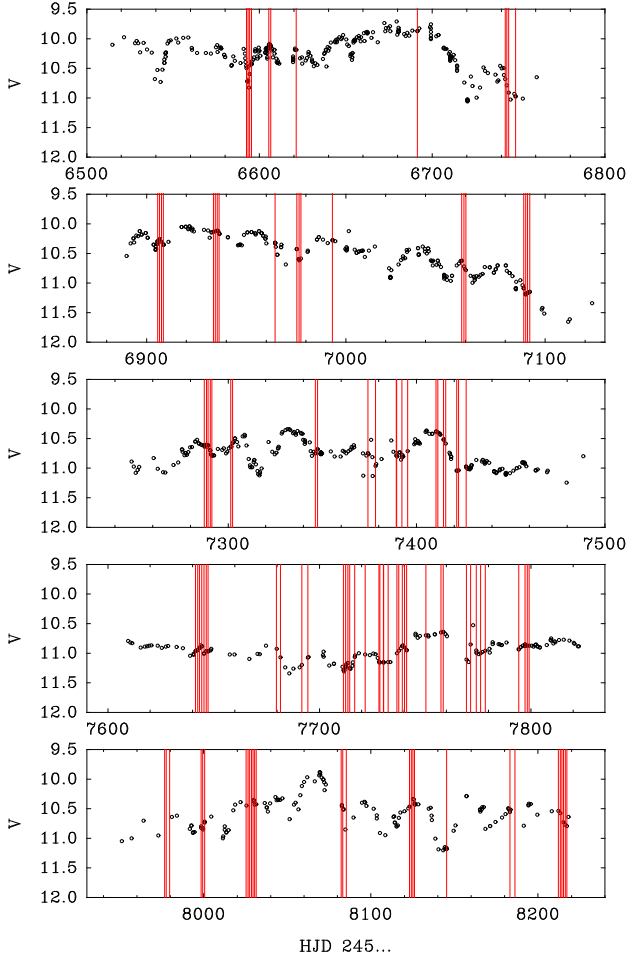


**Figure 1.** Light curves of RY Tau in five seasons, from 2013-2014 (upper panel) to 2017-2018 (lower panel). Vertical lines mark the moments of spectral observations.

the scatter of points in the  $V/(V - R_j)$  diagrams, the error of the unreddened  $V$  may be within 0.10 mag. From these estimates we get the interstellar reddening  $A_V = 0.80 \pm 0.10$  mag for SU Aur and  $A_V = 1.60 \pm 0.10$  mag for RY Tau. These values are consistent with previous estimates of the reddening from optical data (e.g. Calvet et al. 2004; Herczeg & Hillenbrand 2014; Grankin 2017).

The diagrams of RY Tau show a reversal of colours: as the circumstellar extinction gets large, the colour turns bluer. The colour reversal effect is typical for UX Ori type stars: obscuration of star by the circumstellar dust results in increased contribution of the light scattered on the dust particles. This effect was earlier observed in some cTTS, e.g. RY Lup (Gahm et al. 1989, 1993b). In RY Tau we do not see the linear part of the  $V/(B - V)$  diagram but only the curved track. One may suspect that the star still remains obscured by circumstellar dust even at the brightest state. Therefore, in the case of RY Tau, the estimated  $A_V$  may be considered only as an upper limit of interstellar reddening. In SU Aur this effect is normally absent. The resulting stellar parameters are given in Table 1.

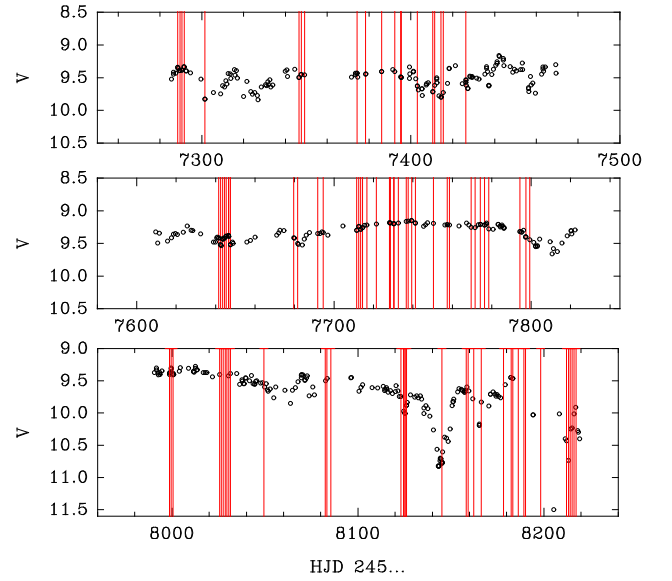


**Figure 2.** Light curves of SU Aur in three seasons, from 2015-2016 (upper panel) to 2017-2018 (lower panel). Vertical lines mark the moments of spectral observations.

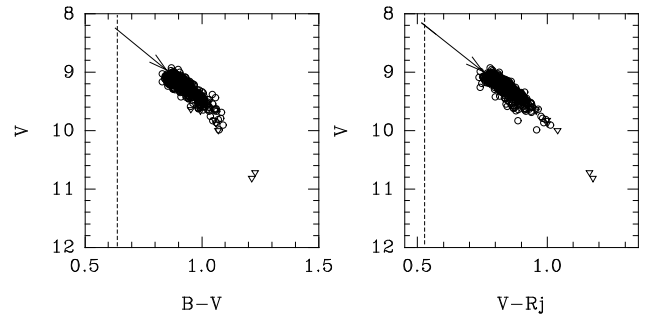


**Figure 3.** Colour-magnitudes diagrams for SU Aur. Open circles - Majdanak data of 1983- 2003. Triangles - CrAO photometry during the minimum of 2017. Arrows indicate the slope of the interstellar reddening. Vertical dashed lines mark the normal colours of a star with  $T_{\text{eff}} = 5945$  K.

The pattern of light variability of RY Tau and SU Aur may be illustrated with the SED in the optical and NIR regions, covered by our photometry (see Tables A3 and A4). We selected a few observations at high and low brightness in the  $V$  band of each star. The corresponding SEDs are shown in Fig. 5 and 6. In both stars the SED is a sum of the stellar radiation reddened by the interstellar and circumstellar extinctions and a black-body radiation of the circumstellar dust. The difference between the two stars is the relative contribution of the stellar and circumstellar radiation. In RY Tau the optical part of the SED is more depressed by the large circumstellar extinction. At minimal brightness the optical SED is more flat because of the light scattered by the

**Table 1.** Stellar parameters of RY Tau and SU Aur.

Star	distance pc	Vmax mag	Av mag	Mv mag	$T_{\text{eff}}^a$ K	$L/L_{\odot}$	$R/R_{\odot}$	$M/M_{\odot}$	Age Myr
RY Tau	$150.0 \pm 10$	9.55	1.60	$2.11 \pm 0.15$	$5945.0 \pm 142.5^a$	$13.50 \pm 1.70$	$3.30 \pm 0.25$	$2.08 \pm 0.10$	$4.70^{+1.00}_{-0.80}$
SU Aur	$142.4 \pm 12$	8.95	0.80	$2.43 \pm 0.18$	$5945.0 \pm 142.5$	$10.09 \pm 1.64$	$2.85 \pm 0.22$	$1.88 \pm 0.10$	$6.60^{+1.04}_{-0.82}$

<sup>a</sup>  $T_{\text{eff}}$  is from [Calvet et al. \(2004\)](#)

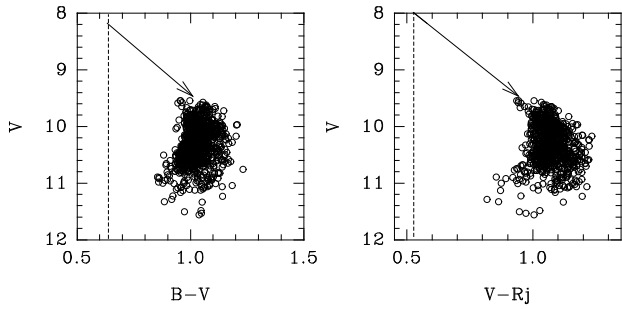


**Figure 4.** Colour-magnitudes diagrams for RY Tau according to Majdanak data of 1984 - 2004. Arrows indicate the slope of the interstellar reddening. Vertical dashed lines mark the normal colours of a star with  $T_{\text{eff}} = 5945$  K.

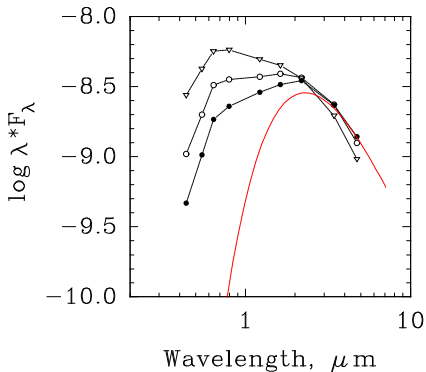


**Figure 5.** Spectral energy distributions (SED) of SU Aur, corresponding to  $V=9.18$  (triangles),  $V=10.00$  (open circles) and  $V=10.72$  (filled circles). Solid curve: SED of a black body at  $T = 1600$  K. Flux  $F_{\lambda}$  is expressed in units of  $\text{erg cm}^{-2} \text{s}^{-1} \text{\AA}^{-1}$ .

circumstellar dust. There is a small but noticeable variability in the NIR part of the SED in both stars.

## 4.2 Spectroscopy

In the analysis of the spectral series we focus on variations of the  $H\alpha$  and Na I D line profiles, which are the strongest indicators of gas flows in the visible region of the spectrum. In addition, some other lines, including photospheric lines, were involved in the analysis. Our spectroscopic series cover a major part of the light variations: from  $V = 9.8$  mag to  $V = 11.2$  mag in RY Tau and from  $V = 9.3$  mag to  $V = 10.8$  mag in SU Aur. In both stars the photospheric spectrum remains unchanged: the depth of the photospheric lines in the region around  $6000\text{\AA}$  at high and low brightness remains

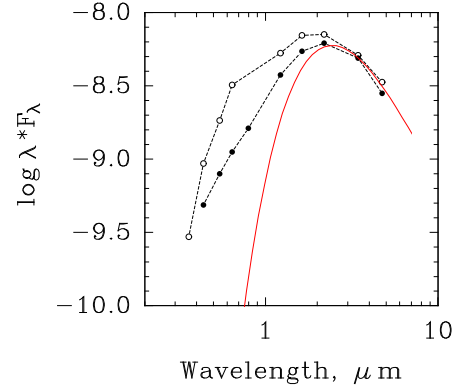


**Figure 6.** Spectral energy distributions in RY Tau, corresponding to  $V=10$  (open circles) and  $V=11$  (filled circles). Solid curve: SED of a black body at  $T=1500$  K. Flux  $F_{\lambda}$  is expressed in units of  $\text{erg cm}^{-2} \text{s}^{-1} \text{\AA}^{-1}$ .

the same within  $\pm 2\%$  of the continuum level. It means that the observed light variations are not related to any surface phenomenon, like hot or cool spots, but are mostly due to variable circumstellar extinction. The stellar radial velocity is  $+18.0 \pm 2.0 \text{ km s}^{-1}$  in both RY Tau and SU Aur, consistent with previous measurements ([Petrov et al. 1996, 1999](#)).

The most evident result is the large variability in  $H\alpha$  and Na I D profiles on a timescale of a day and longer. Samples of typical line profiles in RY Tau are shown in Fig. 7. In this and other diagrams of spectral lines we use astrometric radial velocity scale. The  $H\alpha$  line is in broad emission extending from  $-300$  to  $+300 \text{ km s}^{-1}$ , with a strong "central" depression at about  $-100 \text{ km s}^{-1}$ , which often extends further to the blue and in rare cases drops even below continuum. In terms of line profile classification by [Reipurth et al. \(1996\)](#),  $H\alpha$  is of II-B type most of the time. This is characteristic of an outflow, probably a disc wind ([Kurosawa et al. 2011](#)) or conical wind ([Kurosawa & Romanova 2012](#)). On the other hand, a red-shifted depression in the  $H\alpha$  profile at  $+100$  to  $+200 \text{ km s}^{-1}$  is often present. Comparison of the concurrent  $H\alpha$  and Na I D line profiles in Fig. 7 clearly shows that the depressions in  $H\alpha$  profile correspond to real absorption components in the Na I D lines, although at a lower range of velocities. Therefore, the red-shifted absorption in both lines forms in the infalling gas, most probably in the accretion funnels. These red-shifted absorptions, indicating accretion, are much better seen in the Paschen and Brackett series as real absorption below the continuum (e.g. [Folha & Emerson 2001](#)). In our analysis of the  $H\alpha$  profile variability we study only the outflow activity.

In SU Aur the  $H\alpha$  profiles show similar features of wind and accretion (Fig. 8). The central absorption at about  $-40$

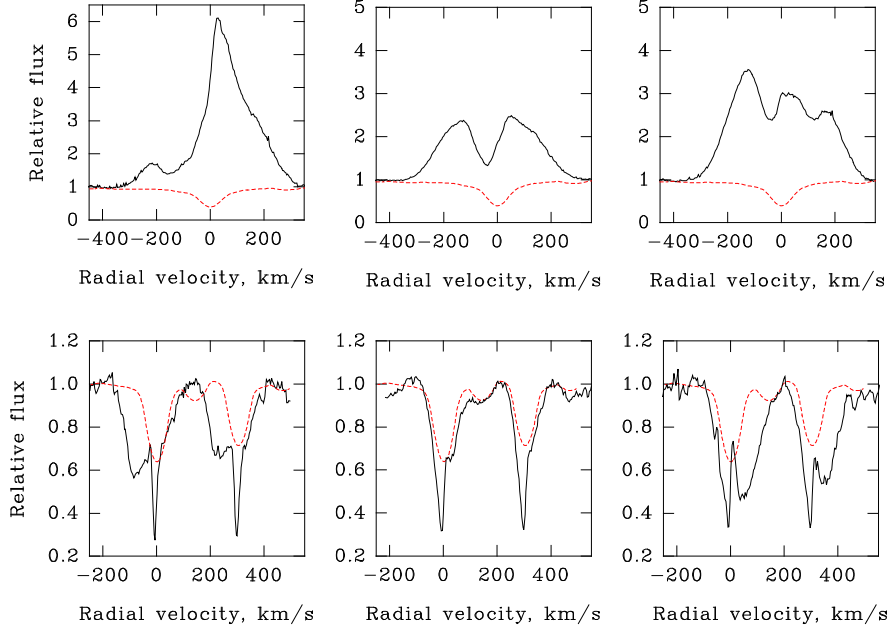


**Figure 7.** Sample of line profiles in RY Tau. Upper panels:  $H\alpha$ , lower panels: Na I D. Left column: HJD=2456993.262, middle: HJD=2457799.442, right: HJD=2457091.204. Dashed curves: template G2 V star,  $v \sin i = 50 \text{ km s}^{-1}$ .

$\text{km s}^{-1}$  is more narrow and deep, and another broader absorption appear sometime at radial velocities of -100 to -250  $\text{km s}^{-1}$ . The same features are present in the Na I D lines, which consist of broad photospheric absorption, narrow interstellar absorption, and the variable blue-shifted absorption indicating outflow.

#### 4.2.1 Spectral series of RY Tau

The  $H\alpha$  emission is an indicator of MHD processes at the boundary between the stellar magnetosphere and the accretion disc. The stellar brightness is related to the amount of dust around the star. In the following analysis we seek for a possible connection between variations in  $H\alpha$  emission and in the circumstellar extinction, i.e. the stellar brightness.

The range of  $H\alpha$  profile variability in RY Tau is shown in Fig. 9. The most variable part of the  $H\alpha$  profile is the central peak of emission at about  $+50 \text{ km s}^{-1}$  and the depression in the blue wing at about  $-100$  to  $-200 \text{ km s}^{-1}$ . In order to quantify the profile variability, we measured equivalent widths (EW) in three ranges of the velocity scale: EWb at  $-200$  to  $-100 \text{ km s}^{-1}$ , EW0 at  $-100$  to  $0 \text{ km s}^{-1}$ , and EWr at  $0$  to  $+100 \text{ km s}^{-1}$ . The ratio EWb/EWr (or EW0/EWr) is a measure of the line asymmetry, caused mostly by the outflow. Fig. 10 shows the relation between the  $H\alpha$  profile asymmetry and stellar brightness  $V$ . In the first two seasons, when the line profile was most variable, there was a clear correlation: the blue wing of  $H\alpha$  emission was depressed at the moments of high brightness of the star. Consequently, the circumstellar extinction was lower during times of enhanced outflow. In the last two seasons, when the activity resumed after the period of quiescence, the most variable part of the line profile shifted to lower velocities, and the ratio EW0/EWr showed a correlation with stellar brightness.

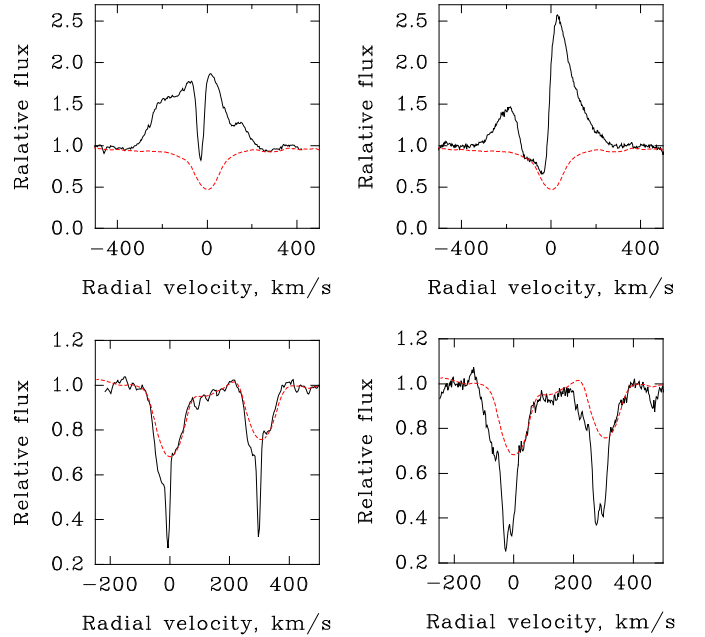


**Figure 8.** Sample of line profiles in SU Aur. Upper panels:  $H\alpha$ , lower panels: Na I D. Left column: HJD=2458030.503, right: HJD=2458166.352. Dashed curves: template G2 V star,  $v \sin i = 66 \text{ km s}^{-1}$ .

#### 4.2.2 Spectral series of SU Aur

SU Aur was monitored only during three seasons. The range of  $H\alpha$  profile variability is shown in Fig. 11. The line is broad with wings extending to radial velocities of about  $\pm$

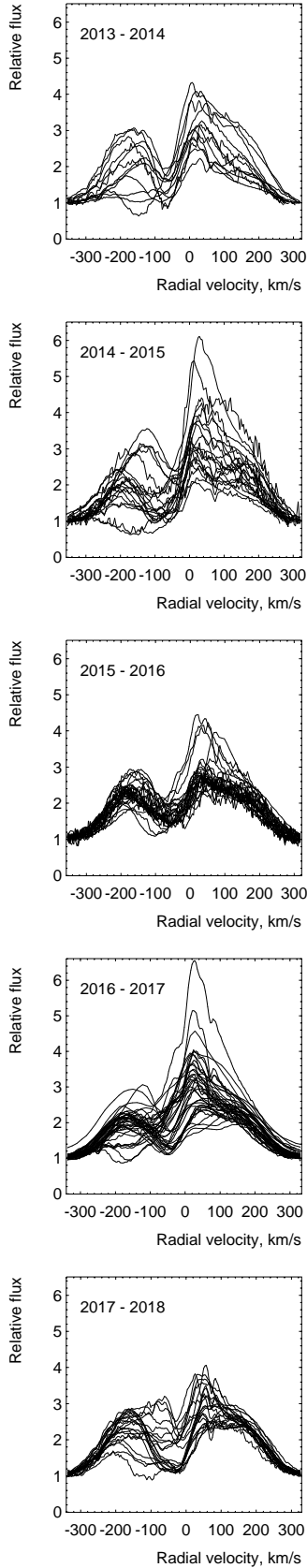


**Figure 9.**  $H\alpha$  profile variation in RY Tau in five seasons as indicated in the upper left corner of each panel. The high activity in 2014-2015 was changed to a period of quiescence in 2015-2016.

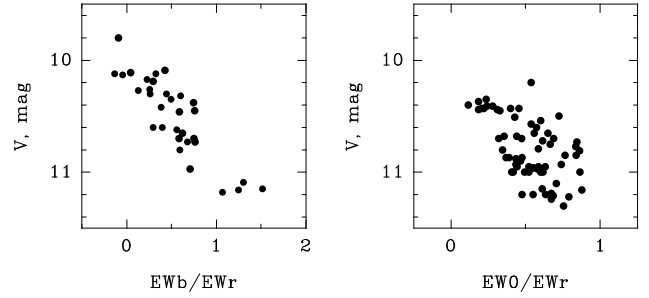


**Figure 10.** Relation between the stellar brightness  $V$  and the  $H\alpha$  line asymmetry. Left: data of 2013-2015, right: data of 2016-2018. The star is brighter when the line asymmetry indicates stronger wind.

$400 \text{ km s}^{-1}$ . On one occasion, the red emission wing extends to almost  $600 \text{ km s}^{-1}$ . Both wings vary in intensity, indicating irregular processes of accretion and outflows. There is a relatively stable narrow absorption at about  $-50 \text{ km s}^{-1}$ . In terms of magnetospheric accretion and disc wind models, it may be identified with absorption in the disc wind or conical wind (Kurosawa et al. 2011; Kurosawa & Romanova 2012).

In the season of 2016-2017 the star showed an unusually low intensity in the  $H\alpha$  emission line. The mean level of stellar brightness did not change considerably in that season, so it was a real decrease in the  $H\alpha$  flux. In the Na I D lines the absorption related to outflow was absent in some nights of that period. Interestingly, that in 2016-2017 the star also showed an unusual low amplitude in the brightness variations (Fig. 2, middle panel). Unlike RY Tau, there is no correlation between the  $H\alpha$  line asymmetry and the stellar brightness in SU Aur.

#### 4.2.3 $H\alpha$ flux variations

So far we analysed  $H\alpha$  equivalent width and the line profile. In the following discussion, an important parameter is the flux radiated in  $H\alpha$ . Our photometry enables to transform the equivalent width of  $H\alpha$  into flux:  $F = EW \times 10^{-0.4(V-V_0)}$ , where  $V_0$  is a reference level of stellar brightness, e.g.  $V_0 = 10$  mag. In this case the flux is expressed in units of the continuum flux density of a star with  $V = 10$  mag, which is  $3.67 \times 10^{-13} \text{ erg cm}^{-2} \text{ s}^{-1} \text{ \AA}^{-1}$ . The photometric R band is more appropriate for  $H\alpha$  flux calibration, but for some spectral observations only  $V$  is available from the AAVSO data. In RY Tau, the colour ( $V - R$ ) does not change considerably with brightness (see Fig. 4). On the average,  $(V - R) = 1.1 \pm 0.1$  mag. The use of  $V$  magnitudes introduces a constant factor to the flux adding a relative error of about 10%. In our analysis, the absolute value of the flux is not critical.

Time variations of the absolute flux in  $H\alpha$  emission line in RY Tau and SU Aur are shown in Fig. 12.

## 5 DISCUSSION

The photometric and spectral properties of RY Tau and SU Aur, discussed in the previous sections, reveal similarities



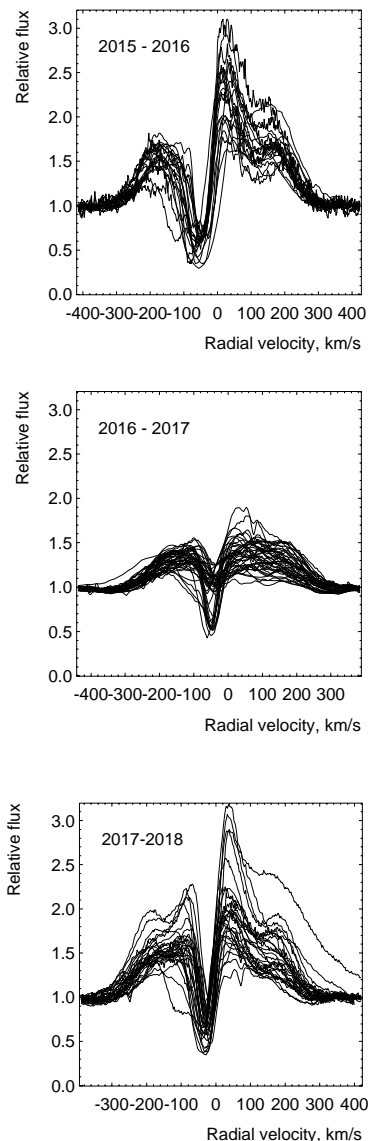


**Figure 11.**  $H\alpha$  profile variation in SU Aur in three seasons. The season of observation is indicated in the upper left corner of each plot.

and differences between the two PMS stars. Stellar parameters are about the same, but RY Tau is younger and more obscured by the circumstellar dust.

The powerful outflows in cTTS are driven by accretion, and the observed variations of the outflows are related to the unstable MHD processes at the boundary between the inner disc and stellar magnetosphere (Zanni & Ferreira 2013). In the observed  $H\alpha$  profiles, the most stable feature is the “central” absorption at  $-100$  to  $-50$  km s $^{-1}$ . This absorption is related to an extended disc wind in the case of high inclinations ( $50^\circ - 80^\circ$ ) of its rotational axis to the line of sight (Kurosawa et al. 2011). The relative stability of this feature is due to a large area along the line of sight above the disc plane, where the absorption is formed. Alternatively, a similar type of profile can be formed in a conical wind starting near the interface of the magnetosphere and the accretion

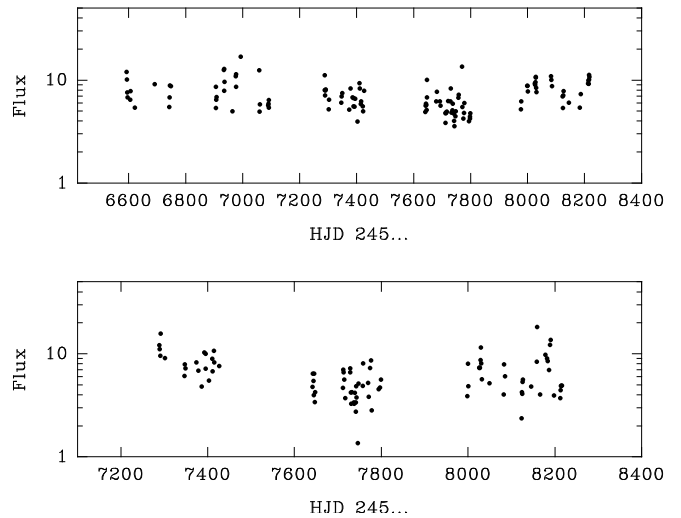


**Figure 12.** Time variations in the absolute flux in  $H\alpha$  emission line. Upper panel: RY Tau, lower panel: SU Aur. Flux is in units of  $3.67 \times 10^{-13}$  erg cm $^{-2}$  s $^{-1}$  Å $^{-1}$ .

disc, when the stellar dipole magnetic field is compressed by the accretion disc into an X-wind like configuration (Kurosawa & Romanova 2012).

More variable is the blue wing of  $H\alpha$  emission at  $-200$  to  $-100$  km s $^{-1}$ . The amplitude of the flux variation in that region is large, including occasional appearance of the classical P Cyg type profile. Such profiles indicate radially expanding outflows, which is drastically different from the disc wind. This fast expansion can be identified with a Magnetospheric Ejection (ME). The MEs appear when the inner disc comes closer to the star and the faster Keplerian rotation twists the stellar magnetosphere in azimuthal direction, which results in cyclically repeated openings and reconstructions of the magnetosphere (Goodson et al. 1997; Zanni & Ferreira 2013).

The wind dynamics and variations in the circumstellar extinction are more evident in RY Tau. This may be a consequence of the higher accretion rate. The mass accretion rate can be estimated from the equivalent widths of the Hydrogen and Helium emission lines, using the empirical relations between line luminosity and mass accretion rate (e.g., Alcalá et al. 2014). We derived the average accretion rates of our targets as:  $\approx 3.6 \times 10^{-8} M_\odot \text{yr}^{-1}$  for RY Tau and  $\approx 4 \times 10^{-9} M_\odot \text{yr}^{-1}$  for SU Aur. This is consistent with the previous determination of the mass accretion rates from optical-UV data on these stars (Calvet et al. 2004).

In the following discussion we consider two topics: 1) influence of the MEs on the dusty disc wind, and 2) the nature of the gradual changes in the wind activity on a time scale of 1-2 years.

### 5.1 Interaction between the wind and the dusty environment

The observed decrease of circumstellar extinction at the moments of the most intensive MEs ( Fig. 10) in RY Tau provides a possibility to localize the dust responsible for the

extinction. Our observations showed that the characteristic radial velocity of the MEs is about  $200 \text{ km s}^{-1}$ , and the characteristic time scale of MEs is about two days (Babina et al. 2016). Then, the typical distance from the expanding magnetosphere to the obscuring dust screen must be about 0.2 AU. Assuming the magnetospheric radius of about 5 stellar radii ( $= 0.08 \text{ AU}$ ) we get the location of the dust screen at about 0.3 AU. This is near the inner edge of the dusty disc, where the dust temperature is high. The SED in the NIR (Fig. 6) shows radiation of dust at  $T=1500 \text{ K}$ . Therefore, this hot dust can be identified as a cause of the variable circumstellar extinction. The star is seen through the dust screen, where the circumstellar extinction on a line of sight is changing, while the bulk radiation from the dust remains relatively constant. Similar effect was observed in another cTTS, namely RW Aur. During a deep minimum of optical brightness of the star the NIR radiation increased, thus indicating appearance of a hot dust (Shenavrin et al. 2015).

An accretion disc is a reservoir of dust. Coarse dust grains are concentrated at the disc plane, while small particles are present in the disc atmosphere and can be elevated from the disc plane by dynamical pressure of the disc wind (Safier 1993). The disc wind is most intensive at the inner part of the disc, where the temperature is higher. Therefore, the most dense dust screen is formed at the inner disc, near the dust sublimation distance and further out from the star.

The disc wind flows along the open magnetic field lines of the disc. The observed correlation between the  $H\alpha$  profile variations and stellar brightness (Fig. 10) implies that there must be a physical mechanism of interaction between the MEs and the dusty disc wind close to the magnetosphere. As a tentative explanation we suggest that a parcel of ionized gas, ejected from magnetosphere can affect the magnetic field of the inner disc and thus temporarily change the disc wind flow on the line of sight.

In RY Tau this effect was more pronounced during the two seasons of maximal activity of magnetospheric ejections in 2013-2015. Then the star entered a period of quiescence, when both the wind activity and the light variations became lower. In the last two seasons the effect appeared again. Since this effect has been observed repeatedly for several years, it can be considered as well established. In SU Aur such a connection between the wind and the circumstellar extinction was not observed.

The colour-magnitude diagrams (Fig. 4) show that RY Tau is permanently hidden by the dust screen, so that the intensity of the light scattered on the dust particles is comparable to the intensity of the direct star light. Contrary to RY Tau, SU Aur is at normal (high) brightness most of the time, but is occasionally obscured by circumstellar dust. This difference may be related to the age: RY Tau is younger and possess a more massive accretion disc (Akeson et al. 2005).

## 5.2 Seasonal changes in outflow activity

Our results show that there is a gradual change of the outflow activity on time scales of a few years. In RY Tau we observed a period of activity in the first two seasons, which was then replaced with a period of quiescence between 2015 and 2016. Although the number of observations in that season were large, the  $H\alpha$  emission showed only a small ampli-

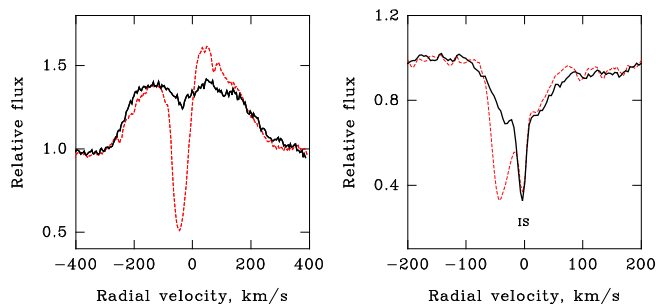


**Figure 13.** Disappearance of the wind features in SU Aur in December 2016. Left:  $H\alpha$ , right : Na I D2. Dashed lines: typical profiles with blue-shifted wind absorptions. Solid lines: spectrum of December 05, 2016. IS: interstellar absorption in the D2 line.

tude of variability. A similar drop of activity was observed in SU Aur between 2016 and 2017. Obviously, in the periods of quiescence the mechanism of ME did not work.

Remarkable is the period of quiescence in SU Aur, when the disc wind became very weak and almost absent. Fig. 13 shows that the usually strong "central" absorption in  $H\alpha$  almost disappeared in December 2016. The corresponding absorption feature in the sodium doublet disappeared completely: the Na I D2 line showed only the broad photospheric absorption and the narrow interstellar feature. The period when the wind was weak started in November 2016 and lasted to the end of the season. In the beginning of the next season (September 2017) the wind was active again. The minimal EW of  $H\alpha$  reached  $0.5 - 1.0 \text{ \AA}$ , and the corresponding accretion rate was less than  $10^{-9} M_{\odot} \text{ yr}^{-1}$ . Interestingly, that during the quiescence period SU Aur was also quiet photometrically, with a minimal circumstellar extinction and low variability within  $V= 9.2 - 9.4$  (See Fig. 2, middle panel).

The outflow is accretion driven, and the region of most unstable outflow is the interface between the disc and stellar magnetosphere. Could the quiescence periods be a consequence of a temporal lowering of accretion rate? The absolute flux in  $H\alpha$  line is often used as a measure of the mass accretion rate. Figure 12 shows that the instant accretion rate is highly variable, while the average level does not change significantly from season to season. From the five seasons of our observations of RY Tau we do not see a correlation between the wind activity and the average  $H\alpha$  flux in a season. The quiescent period in 2015-2016 corresponds to an average level of the  $H\alpha$  flux. In SU Aur we have only three seasons of observations, therefore it is difficult to make a conclusion. The period of quiescence in 2016-2017 corresponds to a slightly lower  $H\alpha$  flux level.

Another important parameter is the stellar magnetic field, which truncates the accretion disc. Zeeman Doppler Imaging of cTTS shows a multipolar structure of magnetic fields (Johnstone et al. 2014 and references therein). Apart from the stellar mass and mass accretion rate, the truncation radius of accretion disc is primarily determined by the strength of the dipole component of the field. If there is solar-like magnetic cycle in cTTS, one would expect cyclic

variations of the disc truncation radius (Johnstone et al. 2014).

Typically, the truncation radius is within the radius of corotation. In this case the inner disc rotates faster than the stellar magnetosphere, and the regime of MEs becomes possible (Zanni & Ferreira 2013). In case of a stronger dipole component of the stellar magnetic field, the disc is truncated outside the corotation radius and the propeller regime is activated (Romanova et al. 2009).

The strength and topology of magnetic field in cTTS vary on a time scale of years (e.g., Donati et al. 2011, 2012). We suggest that the observed changes of the outflow activity in our targets, including the periods of quiescence, may be related to a slow variation of the global stellar magnetic fields, regardless of the type of wind. RY Tau and SU Aur are fast rotating stars with radiative cores and convective envelopes, so the generation of the stellar magnetic field may be similar to the solar one. Spectral monitoring of the H $\alpha$  profile variability in selected cTTS during several years could potentially reveal cycles of magnetic activity, if any.

## 6 CONCLUSIONS

1) RY Tau and SU Aur have about the same stellar parameters, but different circumstellar environment. RY Tau is younger, with the higher accretion rate and a more massive accretion disc. In both stars, the light variability in the optical region is mostly due to the circumstellar extinction.

2) The dusty screen responsible for the variable circumstellar extinction of RY Tau is located at the inner edge of the accretion disc: this is a dusty disc wind. The obscuring dust has a temperature of about 1500 K. The circumstellar extinction in the line of sight is variable, while the NIR radiation from the bulk of the dust remains about the same.

3) In RY Tau the dusty screen permanently obscures the star: the star is never seen free of foreground dust. Unlike RY Tau, SU Aur exhibits a moderate circumstellar extinction most of the time, with rare cases of light drops due to more extinction.

4) In RY Tau we discovered a new effect: during the events of enhanced outflow the circumstellar extinction gets lower. This indicates that outflows may affect the inner dusty wind.

5) In both RY Tau and SU Aur we detected periods of quiescence: lower amplitude variations in the H $\alpha$  line profiles. The quiescence periods lasted for about one year.

## ACKNOWLEDGEMENTS

This research was supported by the RFBR grant 16-02-00140.

Based partly on observations made with the Nordic Optical Telescope, operated by the Nordic Optical Telescope Scientific Association at the Observatorio del Roque de los Muchachos, La Palma, Spain, of the Instituto de Astrofísica de Canarias, using ALFOSC, which is provided by the Instituto de Astrofísica de Andalucía (IAA) under a joint agreement with the University of Copenhagen and NOTSA.

We acknowledge support from a Visitors Program

at the Department of Astronomy at Stockholm University. JFG and RMGA were supported by Fundação para a Ciência e a Tecnologia (FCT) through national funds (UID/FIS/04434/2013) and by FEDER through COMPETE2020 (POCI-01-0145-FEDER-007672). RMGA is supported by the fellowship PD/BD/113745/2015, under the FCT PD Program PhD::SPACE, funded by FCT (Portugal) and POPH/FSE (EC) and by CRUP through a cooperation program (PAULIF: TC-16/17). DEM acknowledges his work as part of the research activity supported by the National Astronomical Research Institute of Thailand (NARIT), Ministry of Science and Technology of Thailand. SYuG was supported in part by the Ministry of Education and Science of Russia (the basic part of the State assignment, RK no. AAAA-A17-117030310283-7) and by the Act no. 211 of the Government of the Russian Federation, agreement âĎŰ 02.A03.21.0006.

We acknowledge with thanks the variable star observations from the AAVSO International Database contributed by observers worldwide and used in this research.

This work has made use of data from the European Space Agency (ESA) mission *Gaia* (<https://www.cosmos.esa.int/gaia>), processed by the *Gaia* Data Processing and Analysis Consortium (DPAC, <https://www.cosmos.esa.int/web/gaia/dpac/consortium>). Funding for the DPAC has been provided by national institutions, in particular the institutions participating in the *Gaia* Multilateral Agreement.

PPP thanks Marina Romanova for valuable comments.

## REFERENCES

- Agra-Amboage V., Dougados C., Cabrit S., Garcia P. J. V., Ferruit P., 2009, *A&A*, **493**, 1029
- Akeson R. L., et al., 2005, *ApJ*, **622**, 440
- Akitaya H., Ikeda Y., Kawabata K. S., Matsuda K., Okazaki A., Seki M., 2009, *A&A*, **499**, 163
- Alcala J. M., et al., 2014, *A&A*, **561**, 2
- Alencar S. H. P., Basri G., 2000, *AJ*, **119**, 1881
- Alonso-Martinez M., Riviere-Marichalar P., Meeus G., Kamp I., Fang M., Podio L., Dent W. R. F., Eiroa C., 2017, *A&A*, **603**, 138
- Ardila D. R., Basri G., Walter F. M., Valenti J. A., Johns-Krull C. M., 2002, *ApJ*, **567**, 1013
- Babina E. V., Artemenko S. A., Petrov P., 2016, *Astron. Rep.*, **42**, 193
- Basri G., Martin E. L., Bertout C., 1991, *A&A*, **252**, 625
- Blandford R. D., Payne D. G., 1982, *MNRAS*, **199**, 883
- Bouvier J., Bertout C., Bouchet P., 1988, *A&AS*, **75**, 1
- Bouvier J., Cabrit S., Fernandez M., Martin E. L., Matthews J. M., 1993, *A&A*, **272**, 176
- Bouvier J., Alencar S. H. P., Harries T. J., Johns-Krull C. M., Romanova M. M., 2007, *Protostars and Planets V*, pp 479–494
- Cabrit S., Edwards S., Strom S. E., Strom K. M., 1990, *ApJ*, **354**, 687
- Calvet N., Muzerolle J., Briceño C., Hernández J., Hartmann L., Saucedo J. L., Gordon K. D., 2004, *AJ*, **128**, 1294
- Camenzind M., 1990, in Klare G., ed., *Reviews in Modern Astronomy Vol. 3, Reviews in Modern Astronomy*. pp 234–265, doi:10.1007/978-3-642-76238-3-17
- Chou M.-Y., et al., 2013, *AJ*, **145**, 108
- Cody A. M., Tayar J., Hillenbrand L., Matthews J. M., Kallinger T., 2013, *AJ*, **145**, 79

- Cranmer S. R., 2009, *ApJ*, **706**, 824
- De Leon J., et al., 2015, *ApJ*, **806**, L10
- DeWarf L. E., Sepinsky J. F., Guinan E. F., Ribas I., Nadalin I., 2003, *ApJ*, **590**, 357
- Donati J. F., et al., 2011, *MNRAS*, **412**, 2454
- Donati J., et al., 2012, *MNRAS*, **425**, 2948
- Elias J. H., 1978, *ApJ*, **224**, 857
- Folha D. F. M., Emerson J. P., 2001, *A&A*, **365**, 90
- Furlan E., et al., 2011, *ApJS*, **195**, 3
- Gahm G. F., Fischerstrom C., Liseau R., Lindroos K. P., 1989, *A&AS*, **211**, 115
- Gahm G. F., Gullbring E., Fischerstrom C., Lindroos K. P., Loden K., 1993a, *A&AS*, **100**, 371
- Gahm G. F., Liseau R., Gullbring E., Hartstein D., 1993b, *A&AS*, **279**, 477
- Ghosh P., Lamb F. K., 1979, *ApJ*, **234**, 296
- Giampapa M. S., Basri G. S., Johns C. M., Imhoff C., 1993, *ApJS*, **89**, 321
- Gomez de Castro A. I., Marcos-Arenal P., 2012, *ApJ*, **749**, 190
- Gomez de Castro A. I., Verdugo E., 2007, *ApJ*, **654**, L91
- Goodson A. P., Winglee R. M., Böhm K.-H., 1997, *ApJ*, **489**, 199
- Grankin K. N., 2017, *ASP Conf. Ser.*, **37**, 511
- Grankin K. N., Melnikov S. Y., Bouvier J., Herbst W., Shevchenko V. S., 2007, *A&A*, **461**, 183
- Grinin V. P., Tambovtseva L. V., Weigelt G., 2012, *A&A*, **544**, A45
- Guilloteau S., Dutrey A., Piétu V., Boehler Y., 2011, *A&A*, **529**, A105
- Hamann F., Persson S. E., 1992, *ApJS*, **82**, 247
- Hartigan P., Edwards S., Ghandour L., 1995, *ApJ*, **452**, 736
- Hartmann L., Herczeg G., Calvet N., 2016, *ARA&A*, **54**, 135
- Herbst W., Koret D. L., 1988, *AJ*, **96**, 1949
- Herbst W., Shevchenko V. S., 1999, *AJ*, **118**, 1043
- Herbst W., Stine P. C., 1984, *AJ*, **89**, 1716
- Herbst W., et al., 1987, *AJ*, **94**, 137
- Herbst W., Herbst D. K., Grossman E. J., Weinstein D., 1994, *AJ*, **108**, 1906
- Herczeg G. J., Hillenbrand L. A., 2014, *ApJ*, **786**, 97
- Isella A., Carpenter J. M., Sargent A. I., 2010, *ApJ*, **714**, 1746
- Ismailov N. Z., Adigezalzade H. N., Bahaddinova G. R., 2015, *Publication of Korean Astronomical Society*, **30**, 229
- Jeffers S. V., Min M., Canovas H., Rodenhuis M., Keller C. U., 2014, *A&A*, **561**, A23
- Johns C. M., Basri G., 1995, *AJ*, **109**, 2800
- Johns-Krull C. M., 1996, *A&A*, **306**, 803
- Johnson H. L., Mitchell R. I., Iriarte B., Wisniewski W. Z., 1966, *Communications of the Lunar and Planetary Laboratory*, **4**, 99
- Johnstone C. P., Jardine M., Gregory S. G., Donati J. F., Hussain G., 2014, *MNRAS*, **437**, 3202
- Kafka S., 2017, in *Observations from the AAVSO International Database*, <https://www.aavso.org>
- Kenyon S. J., Hartmann L., 1995, *ApJS*, **101**, 117
- Koenigl A., 1991, *ApJ*, **370**, L39
- Koornneef J., 1983, *A&A*, **128**, 84
- Kurosawa R., Romanova M. M., 2012, *MNRAS*, **426**, 2901
- Kurosawa R., Harries T. J., Symington N. H., 2005, *MNRAS*, **358**, 671
- Kurosawa R., Romanova M. M., Harries T. J., 2011, *MNRAS*, **416**, 2623
- Loinard L., Torres R. M., Mioduszewski A. J., Rodríguez L. F., González-Lópezlira R. A., Lachaume R., Vázquez V., González E., 2007, *ApJ*, **671**, 546
- Matt S., Pudritz R. E., 2005, *ApJ*, **632**, L135
- Mendigutía I., Eiroa C., Montesinos B., Mora A., Oudmaijer R. D., Merín B., Meeus G., 2011, *A&A*, **529**, A34
- Millan-Gabet R., Malbet F., Akeson R., Leinert C., Monnier J., Waters R., 2007, *Protostars and Planets V*, pp 539–554
- Muzerolle J., Calvet N., Hartmann L., D’Alessio P., 2003, *ApJ*, **597**, L149
- Nguyen D. C., Brandeker A., van Kerkwijk M. H., Jayawardhana R., 2012, *ApJ*, **745**, 119
- Oliveira J. M., Foing B. H., van Loon J. T., Unruh Y. C., 2000, *A&A*, **362**, 615
- Panchuk V. E., Yushkin M. V., Yakopov M. V., 2011, *Astrophysical Bulletin*, **66**, 355
- Petrov P. P., 1990, *Ap&SS*, **169**, 61
- Petrov P. P., 2003, *Astrophysics*, **46**, 506
- Petrov P. P., Gullbring E., Ilyin I., Gahm G. F., Tuominen I., Hackman T., Loden K., 1996, *A&A*, **314**, 821
- Petrov P. P., Zajtseva G. V., Efimov Y. S., Duemmler R., Ilyin I. V., Tuominen I., Shcherbakov V. A., 1999, *A&A*, **341**, 553
- Pudritz R. E., Norman C. A., 1986, *ApJ*, **301**, 571
- Reipurth B., Pedrosa A., Lago M. T. V. T., 1996, *A&AS*, **120**, 229
- Romanova M. M., Owocki S. P., 2015, *Space Sci. Rev.*, **191**, 339
- Romanova M. M., Long M., Kulkarni A. K., Kurosawa R., Ustyugova G. V., Koldoba A. K., Lovelace R. V. E., 2007, in *Bouvier J., Appenzeller I., eds, IAU Symposium Vol. 243, Star-Disk Interaction in Young Stars*. pp 277–290 ([arXiv:0803.2865](https://arxiv.org/abs/0803.2865)), [doi:10.1017/S1743921307009635](https://doi.org/10.1017/S1743921307009635)
- Romanova M. M., Ustyugova G. V., Koldoba A. V., Lovelace R. V. E., 2009, *MNRAS*, **399**, 1802
- Safier P. N., 1993, *ApJ*, **408**, 115
- Scheegerer A. A., Wolf S., Ratzka T., Leinert C., 2008, *A&A*, **478**, 779
- Shenavrin V. I., Taranova O. G., Nadzhip A. E., 2011, *Astronomy Reports*, **55**, 31
- Shenavrin V. I., Petrov P. P., Grankin K. N., 2015, *Information Bulletin on Variable Stars*, **6143**, 1
- Shu F., Najita J., Ostriker E., Wilkin F., Ruden S., Lizano S., 1994, *ApJ*, **429**, 781
- Siess L., Dufour E., Forestini M., 2000, *A&A*, **358**, 593
- Skinner S. L., Audard M., Gudel M., 2016, *ApJ*, **826**, 84
- Skinner G. L., Schneider P. C., Audard M., Gudel M., 2018, *ApJ*, **855**, 143
- Smith K. W., Lewis G. F., Bonnell I. A., Bunclark P. S., Emerson J. P., 1999, *MNRAS*, **304**, 367
- Smith K., Audard M., Gudel M., Skinner S., Pallavicini R., 2005, in *Favata F., Hussain G. A. J., Battrick B., eds, ESA Special Publication Vol. 560, 13th Cambridge Workshop on Cool Stars, Stellar Systems and the Sun*. p. 971
- St-Onge G., Bastien P., 2008, *ApJ*, **674**, 1032
- Takami M., et al., 2013, *ApJ*, **772**, 145
- Unruh Y. C., Solanki S. K., Fligge M., 2000, *Space Sci. Rev.*, **94**, 145
- Unruh Y. C., et al., 2004, *MNRAS*, **348**, 1301
- Vink J. S., Drew J. E., Harries T. J., Oudmaijer R. D., Unruh Y., 2005, *MNRAS*, **359**, 1049
- Zajtseva G. V., 2010, *Astrophysics*, **53**, 212
- Zajtseva G. V., Kolotilov E. A., Petrov P. P., Tarasov A. E., Shenavrin V. I., Shcherbakov A. G., 1985, *Pisma v Astronomicheskii Zhurnal*, **11**, 271
- Zajtseva G., Petrov P., Ilyin I., Duemler R., Tuominen I., 1996, *Information Bulletin on Variable Stars*, **4408**
- Zanni C., Ferreira J., 2013, *A&A*, **550**, A99

**APPENDIX A: OBSERVATION DATA**

This paper has been typeset from a  $\text{\TeX/L\AA\TeX}$  file prepared by the author.

**Table A1.** RY Tau V-magnitudes for the dates of spectral observations. The Heliocentric Julian Date (HJD) in the first column is followed by the site of the observation (CAHA - Calar Alto Observatory, CrAO - Crimean Astrophysical Observatory, NOT - Nordic Optical Telescope, TNO - Thai National Observatory), magnitude measured in the V-band, corresponding error and source (CAS - Crimean Astronomical Station, AAVSO - American Association of Variable Star Observers, Int - value interpolated from AAVSO and CrAO photometry).

HJD-2400000	Site	V	V error	Source of V	HJD-2400000	Site	V	V error	Source of V
56592.444	CrAO	10.46	0.01	CrAO	57647.424	CrAO	10.97	0.01	CrAO
56593.438	CrAO	10.70	0.01	CrAO	57679.618	NOT	10.93	<0.01	AAVSO
56594.340	CrAO	10.45	0.01	CrAO	57681.607	NOT	11.07	0.10	Int
56595.306	CrAO	10.38	0.01	CrAO	57691.681	NOT	11.20	0.10	Int
56605.436	CrAO	10.09	0.01	CrAO	57694.607	NOT	11.06	0.02	AAVSO
56606.442	CrAO	10.11	0.01	CrAO	57711.424	CrAO	11.31	0.01	CrAO
56621.318	CrAO	10.19	0.01	CrAO	57712.387	CrAO	11.22	0.01	CrAO
56691.389	CrAO	9.87	0.01	AAVSO	57713.442	CrAO	11.16	0.01	CrAO
56742.224	CrAO	10.68	0.10	Int	57714.418	CrAO	11.27	0.01	CrAO, CAS
56743.185	CrAO	10.79	0.10	Int	57716.650	NOT	11.04	0.02	AAVSO
56744.242	CrAO	10.91	0.10	Int	57721.578	NOT	11.02	0.10	Int
56748.291	CrAO	10.97	0.01	CrAO	57728.594	NOT	11.16	0.01	CrAO, CAS
56905.524	CrAO	10.29	0.01	CrAO	57730.459	NOT	11.15	0.01	CrAO
56906.520	CrAO	10.26	0.01	CrAO	57732.546	NOT	11.15	0.10	Int
56907.504	CrAO	10.30	0.10	Int	57736.650	NOT	10.950	0.01	CAS
56908.509	CrAO	10.35	0.01	CrAO	57737.553	NOT	10.96	0.01	CAS
56933.513	CrAO	10.13	0.10	Int	57741.072	TNO	10.95	0.01	CrAO, CAS
56934.475	CrAO	10.13	0.10	Int	57742.091	TNO	10.90	0.10	Int
56935.416	CrAO	10.12	0.01	CrAO	57743.237	TNO	10.83	0.10	Int
56936.415	CrAO	10.17	0.01	CrAO	57746.144	TNO	10.74	0.01	CrAO, CAS
56964.464	CrAO	10.32	0.01	CrAO	57747.137	TNO	10.71	0.01	CrAO, CAS
56975.442	CrAO	10.42	0.01	CrAO	57752.570	CAHA	10.70	0.10	Int
56976.453	CrAO	10.60	0.01	CrAO	57753.464	CAHA	10.69	0.10	Int
56977.468	CrAO	10.58	0.10	Int	57754.497	CAHA	10.68	0.04	AAVSO
56993.262	CrAO	10.27	0.01	CrAO	57757.407	NOT	10.63	0.01	CAS
57058.188	CrAO	10.62	0.01	CrAO	57758.545	NOT	10.64	<0.01	AAVSO
57059.231	CrAO	10.76	0.01	AAVSO	57769.523	NOT	11.11	0.10	Int
57060.188	CrAO	10.78	0.10	Int	57771.485	NOT	10.85	0.10	Int
57089.231	CrAO	11.09	0.01	CrAO	57774.159	CrAO	10.99	0.01	CrAO
57090.203	CrAO	11.18	0.01	CrAO	57776.205	CrAO	11.00	0.10	Int
57091.204	CrAO	11.16	0.02	CrAO	57778.447	NOT	10.95	0.10	Int
57092.230	CrAO	11.15	0.08	CrAO	57794.194	CrAO	10.93	0.01	CrAO
57287.438	CrAO	10.61	0.01	CrAO	57797.186	CrAO	10.85	0.01	CrAO, CAS
57288.532	CrAO	10.61	0.01	CrAO	57798.200	CrAO	10.87	0.10	Int
57289.438	CrAO	10.61	0.01	CrAO	57799.180	CrAO	10.87	0.10	Int
57290.511	CrAO	10.69	0.01	CrAO	57998.442	CrAO	10.82	0.01	CrAO
57291.444	CrAO	10.78	0.01	CrAO	57999.442	CrAO	10.85	0.01	CrAO
57301.430	CrAO	10.64	0.01	CrAO	58000.445	CrAO	10.72	0.01	CrAO
57302.482	CrAO	10.56	0.01	AAVSO	58025.441	CrAO	10.45	0.01	CrAO
57346.369	CrAO	10.75	0.01	CrAO	58026.483	CrAO	10.42	0.10	Int
57347.483	CrAO	10.68	0.01	CrAO	58027.476	CrAO	10.40	0.10	Int
57349.166	TNO	10.75	0.01	AAVSO	58028.475	CrAO	10.38	0.10	Int
57374.180	CrAO	10.74	0.01	CrAO	58029.435	CrAO	10.37	0.01	CAS
57378.300	CrAO	10.93	0.01	CrAO	58030.438	CrAO	10.43	0.01	CAS
57386.009	TNO	10.53	<0.01	AAVSO	58031.438	CrAO	10.43	0.01	CAS
57389.298	CrAO	10.80	0.01	AAVSO	58082.248	CrAO	10.45	0.01	CrAO
57389.413	CAHA	10.80	0.01	AAVSO	58083.247	CrAO	10.51	0.01	CrAO
57392.334	CrAO	10.78	0.01	CrAO	58085.234	CrAO	10.83	0.10	Int
57403.056	TNO	10.50	0.10	Int	58123.148	CrAO	10.46	0.01	CAS
57410.370	CAHA	10.38	<0.01	AAVSO	58124.275	CrAO	10.37	0.10	Int
57411.368	CAHA	10.40	0.10	Int	58125.149	CrAO	10.34	0.01	CrAO
57414.380	CAHA	10.52	0.01	CrAO, CAS	58126.144	CrAO	10.41	0.01	CrAO, CAS
57415.458	CAHA	10.59	0.10	Int	58145.229	CrAO	11.18	0.01	CrAO, CAS
57421.302	CrAO	11.04	0.01	CrAO	58183.200	CrAO	10.55	0.01	CrAO
57422.315	CrAO	11.04	0.10	Int	58186.251	CrAO	-	-	-
57426.327	CrAO	10.98	0.01	CrAO	58212.224	CrAO	10.54	0.01	CrAO
57641.426	CrAO	10.96	0.01	CrAO, CAS	58213.225	CrAO	10.57	0.01	CrAO
57642.442	CrAO	10.95	0.01	CrAO	58214.217	CrAO	10.65	0.10	Int
57643.418	CrAO	10.91	0.01	CrAO, CAS	58215.220	CrAO	10.73	0.01	CrAO
57644.402	CrAO	10.88	0.01	CrAO	58216.215	CrAO	10.77	0.01	CrAO
57645.393	CrAO	11.01	0.01	CrAO	58217.219	CrAO	10.79	0.01	CrAO
57646.416	CrAO	10.96	0.01	CrAO					

**Table A2.** *SU Aur* V-magnitudes for the dates of spectral observations. The Heliocentric Julian Date (HJD) in the first column is followed by the site of the observation (CAHA - Calar Alto Observatory, CrAO - Crimean Astrophysical Observatory, NOT - Nordic Optical Telescope, TNO - Thai National Observatory, UrFU - Kourovka Astronomical Observatory), magnitude measured in the V-band, corresponding error and source (CAS - Crimean Astronomical Station, AAVSO - American Association of Variable Star Observers, Int - value interpolated from AAVSO and CrAO photometry).

HJD-2400000	Site	V	V error	Source of V	HJD-2400000	Site	V	V error	Source of V
57288.462	CrAO	9.34	0.01	CrAO	57778.455	NOT	9.22	0.10	Int
57289.503	CrAO	9.39	0.01	CrAO	57794.263	CrAO	9.32	0.01	CrAO
57290.490	CrAO	9.39	0.01	CrAO	57797.259	CrAO	9.40	0.01	CrAO
57291.502	CrAO	9.33	0.01	CrAO	57799.248	CrAO	9.44	0.10	Int
57301.500	CrAO	9.83	0.01	CrAO	57998.513	CrAO	9.40	0.01	CrAO
57346.440	CrAO	9.50	0.01	CrAO	57999.509	CrAO	9.30	0.01	CrAO
57347.510	CrAO	9.45	0.01	CrAO	58000.510	CrAO	9.39	0.01	CrAO
57349.190	TNO	9.46	0.10	Int	58025.536	CrAO	9.41	0.01	CrAO
57374.225	CrAO	9.43	0.01	CrAO	58026.549	CrAO	9.40	0.10	Int
57378.333	CrAO	9.44	0.01	CrAO	58027.542	CrAO	9.40	0.10	Int
57386.090	TNO	9.40	0.10	Int	58028.540	CrAO	9.40	0.10	Int
57392.351	CrAO	9.41	0.10	Int	58029.500	CrAO	9.40	0.10	Int
57395.086	TNO	9.50	0.01	AAVSO	58030.503	CrAO	9.43	0.01	CAS
57395.406	CAHA	9.50	0.01	AAVSO	58031.502	CrAO	9.39	0.01	CAS
57403.076	TNO	9.69	<0.01	AAVSO	58049.473	UrFU	9.60	0.01	AAVSO
57410.402	CAHA	9.72	0.01	AAVSO	58082.322	CrAO	9.50	0.01	CrAO
57411.401	CAHA	9.61	0.10	Int	58083.312	CrAO	9.46	0.01	CrAO
57414.412	CAHA	9.80	0.01	CrAO	58085.302	CrAO	9.46	0.10	Int
57415.489	CAHA	9.73	0.10	Int	58123.193	CrAO	9.74	0.01	CAS
57426.373	CrAO	9.53	0.01	CrAO	58124.482	UrFU	9.98	0.01	AAVSO
57641.536	CrAO	9.42	0.01	CrAO	58125.216	CrAO	10.01	0.01	CrAO
57642.517	CrAO	9.52	0.01	CrAO	58125.404	UrFU	10.01	0.01	CAS
57643.524	CrAO	9.43	0.01	CrAO	58126.210	CrAO	9.88	0.01	CrAO
57644.467	CrAO	9.41	0.01	CrAO	58145.165	CrAO	10.76	0.01	CAS
57645.460	CrAO	9.39	0.01	CrAO	58158.293	UrFU	9.60	0.01	AAVSO
57646.481	CrAO	9.38	0.01	CrAO	58159.324	UrFU	9.66	0.01	AAVSO
57646.689	NOT	9.38	0.01	CrAO	58162.338	NOT	9.62	0.10	Int
57647.490	CrAO	9.52	0.01	CrAO	58182.355	CrAO	9.45	0.01	CrAO
57679.623	NOT	9.42	<0.01	AAVSO	58183.266	CrAO	9.47	0.01	CrAO
57681.613	NOT	9.51	0.01	AAVSO	58186.225	CrAO	9.62	0.10	Int
57691.688	NOT	9.35	0.10	Int	58212.262	CrAO	10.43	0.01	CrAO
57694.614	NOT	9.33	0.10	Int	58213.270	CrAO	10.74	0.01	CrAO
57711.499	CrAO	9.30	0.01	CrAO	58214.242	CrAO	10.27	0.07	AAVSO
57712.584	CrAO	9.24	0.01	CrAO	58215.265	CrAO	10.23	0.01	CrAO
57713.599	CrAO	9.28	0.01	CrAO	58216.260	CrAO	10.01	0.01	CrAO
57714.486	CrAO	9.26	0.01	CrAO					
57716.662	NOT	9.22	0.10	Int					
57721.584	NOT	9.20	0.10	Int					
57728.213	CrAO	9.18	0.01	CrAO					
57728.600	NOT	9.18	0.01	CrAO					
57730.237	CrAO	9.20	0.01	CrAO					
57730.465	NOT	9.20	0.01	CrAO					
57732.643	NOT	9.19	0.10	Int					
57735.584	CAHA	9.17	0.10	Int					
57736.656	NOT	9.16	0.10	Int					
57737.560	NOT	9.16	0.10	Int					
57739.388	CrAO	9.15	0.01	CrAO					
57741.072	TNO	9.19	0.01	CrAO					
57742.091	TNO	9.20	0.10	Int					
57743.237	TNO	9.21	0.10	Int					
57746.144	TNO	9.21	0.01	CrAO					
57747.135	TNO	9.18	0.01	CrAO					
57752.617	CAHA	9.20	0.10	Int					
57753.509	CAHA	9.21	0.10	Int					
57754.547	CAHA	9.21	0.10	Int					
57757.413	NOT	9.21	0.01	CrAO					
57758.551	NOT	9.22	0.10	Int					
57769.537	NOT	9.22	0.10	Int					
57771.491	NOT	9.21	0.10	Int					
57774.232	CrAO	9.21	0.01	CrAO					
57776.273	CrAO	9.22	0.01	CrAO					

**Table A3.** RY Tau photometry. The values corresponding to the UBVRI photometry, taken between 1981 and 1997, are from the Majdanak archive ([Grankin et al. 2007](#)). All the JHKLM magnitudes were obtained at the Crimean Astronomical Station (CAS). The BVRI data correspondent to the period 2013-2018 were obtained at CrAO.

HJD-2400000	U	B	V	R	I	J	H	K	L	M
44888.400	...	...	...	...	...	7.80	6.65	5.55	...	...
44892.400	...	...	...	...	...	7.73	6.60	5.51	...	...
44902.600	...	...	...	...	...	7.78	...	5.61	...	...
46692.400	11.97	11.40	10.24	9.02	...	7.26	6.17	5.26	4.16	...
46694.386	11.90	11.29	10.15	8.95	...	7.34	6.19	5.25	4.08	3.74
47053.500	...	...	...	...	...	7.02	6.05	5.24	4.07	3.68
47126.500	...	...	...	...	...	7.26	6.24	5.35	...	3.65
47569.300	...	...	...	...	...	6.99	5.99	5.32	4.17	3.80
47825.369	11.81	11.20	10.09	8.96	...	7.15	6.12	5.26	4.09	3.70
50430.400	...	...	...	...	...	6.95	6.03	5.28	4.25	...
50484.300	...	...	...	...	...	6.88	5.92	5.39	4.21	3.82
57289.431	...	11.66	10.61	9.58	8.70	7.37	6.37	5.41	...	...
57291.500	...	11.84	10.78	9.72	8.80	7.47	6.40	5.44	4.23	3.88
57385.300	...	...	...	...	...	7.34	6.37	5.48	4.30	4.03
57391.291	...	11.77	10.73	9.66	8.76	7.36	6.39	5.47	4.31	4.09
57408.263	...	11.44	10.42	9.38	8.51	7.22	6.26	5.38	4.16	3.84
57427.300	...	11.93	11.01	10.06	9.16	7.52	6.39	5.41	4.14	3.89
57444.193	...	11.99	11.04	10.06	9.17	7.61	6.42	5.55	4.23	3.98
57453.200	...	11.89	11.00	10.04	9.20	7.60	6.45	5.41	4.16	3.91
57620.486	...	11.82	10.86	9.85	8.97	7.51	6.46	5.50	4.26	4.07
57623.500	...	11.84	10.87	9.85	8.95	7.51	6.45	5.46	4.20	4.11
57635.464	...	11.96	10.91	9.83	8.94	7.58	6.54	5.56	4.30	3.96
57638.500	...	...	...	...	...	7.61	6.52	5.53	4.25	3.92
57641.488	...	11.99	10.96	9.90	8.99	7.60	6.52	5.52	4.28	3.94
57648.492	...	11.91	10.95	9.93	9.09	7.68	6.59	5.57	4.27	3.92
57680.478	...	11.93	10.94	9.86	8.92	7.43	6.36	5.38	4.19	3.98
57704.400	...	12.08	11.21	10.15	9.27	7.68	6.55	5.50	4.19	4.03
57730.332	...	12.21	11.15	10.06	9.13	7.61	6.51	5.44	4.17	3.68
57745.300	...	11.80	10.68	9.50	8.57	7.30	6.28	5.39	4.11	3.80
57746.216	...	11.86	10.72	9.56	8.63	7.28	6.30	5.35	4.06	3.80
57767.208	...	12.21	11.12	9.97	9.02	7.54	6.43	5.44	4.15	3.98
57774.297	...	12.12	10.99	...	8.93	7.45	6.37	5.39	4.17	3.88
57777.200	...	...	...	...	...	7.53	6.42	5.41	4.15	4.01
57784.185	...	11.90	10.87	9.80	8.90	7.45	6.42	5.44	4.24	3.97
57785.272	...	11.95	10.85	...	...	7.41	6.38	5.44	4.20	4.02
57786.162	...	11.92	10.86	9.75	8.83	7.39	6.38	5.45	4.20	3.99
57795.200	...	11.93	10.90	9.80	8.85	7.33	6.31	5.37	4.13	3.88
57801.278	...	11.88	10.89	9.83	8.93	7.47	6.44	5.45	4.20	3.78
57803.189	...	11.86	10.88	9.88	9.05	7.56	6.48	5.51	4.20	3.88
57812.200	...	11.84	10.79	9.69	8.76	7.45	6.47	5.54	4.28	3.97
57813.226	...	11.84	10.78	9.68	8.76	7.39	6.38	5.52	4.21	3.94
57817.202	...	...	...	...	...	7.34	6.34	5.46	4.23	3.94
57998.512	...	11.85	10.81	9.67	8.76	7.42	6.42	5.49	4.31	3.95
58006.541	...	...	...	...	...	7.36	6.37	5.43	4.26	4.06
58026.513	...	...	...	...	...	7.20	6.28	5.42	4.20	3.88
58030.448	...	...	...	...	...	7.17	6.25	5.39	4.23	3.89
58038.489	...	...	...	...	...	7.24	6.32	5.43	4.27	3.97
58066.397	...	...	...	...	...	7.03	6.17	5.36	4.18	3.96
58096.465	...	11.43	10.40	9.29	8.44	7.22	6.32	5.44	4.20	3.95
58100.320	...	...	...	...	...	7.30	6.36	5.46	4.23	3.96
58114.436	...	11.78	10.73	9.65	8.75	7.29	6.34	5.38	4.10	3.62
58116.293	...	...	...	...	...	7.43	6.41	5.44	4.20	3.93
58120.251	...	...	...	...	...	7.23	6.25	5.36	4.19	3.90
58125.437	...	11.44	10.34	9.23	8.34	7.10	6.19	5.34	4.21	3.95
58126.210	...	11.54	10.41	9.29	8.39	7.14	6.23	5.36	4.19	3.91
58143.219	...	...	...	...	...	7.46	6.47	5.51	4.22	3.84
58145.209	...	...	...	...	...	7.46	6.45	5.48	4.28	4.03
58151.178	...	...	...	...	...	7.31	6.34	5.44	4.24	4.00



**Table A4.** *SU Aur* photometry. All the JHKLM magnitudes were obtained at the Crimean Astronomical Station (CAS). The BVRI data correspondent to the period 2013-2018 were obtained at CrAO.

HJD-2400000	B	V	R	I	J	H	K	L	M
57313.551	10.40	9.44	8.54	7.95	7.35	6.69	6.00	5.14	4.74
57324.290	10.77	9.75	8.79	8.11	7.47	6.77	6.02	5.06	4.80
57391.301	10.30	9.38	8.49	7.92	...	...	5.99	5.12	4.98
57399.372	10.27	9.34	8.44	7.91	7.36	6.67	6.03	5.12	4.99
57426.268	10.53	9.53	8.64	8.03	7.36	6.65	6.01	5.05	4.78
57623.524	10.16	9.33	8.42	7.86	7.27	6.57	5.94	5.05	5.16
57635.600	...	...	...	...	7.25	6.59	5.96	5.11	4.91
57638.500	...	...	...	...	7.32	6.66	6.02	5.13	4.86
57641.504	10.23	9.42	8.46	7.88	7.31	6.62	5.98	5.12	4.89
57648.474	10.35	9.48	8.51	7.95	7.37	6.69	6.02	5.12	4.92
57680.500	...	...	...	...	7.26	6.56	5.87	4.99	4.81
57704.600	10.10	9.23	8.38	7.83	7.22	6.54	5.92	5.08	4.99
57730.327	10.08	9.20	8.39	7.85	7.23	6.60	5.93	5.06	4.87
57745.456	10.08	9.24	8.40	7.84	7.30	6.72	6.08	5.23	5.03
57746.448	10.06	9.21	8.42	7.86	7.31	6.69	6.07	5.21	5.07
57774.399	10.02	9.21	8.36	7.82	7.26	6.67	6.05	5.18	4.98
57777.256	10.02	9.19	8.35	7.78	7.22	6.60	5.99	5.13	5.04
57785.257	10.04	9.22	8.37	7.83	7.28	6.66	6.04	5.20	5.10
57786.265	10.10	9.25	8.41	7.86	7.31	6.68	6.06	5.20	5.06
57795.232	10.17	9.33	8.44	7.89	7.38	6.72	6.02	5.19	5.00
57803.187	10.46	9.53	8.59	8.01	7.42	6.73	6.04	5.14	5.05
57812.300	...	...	...	...	7.44	6.76	6.07	5.14	5.06
57817.264	...	...	...	...	7.34	6.69	6.04	5.12	4.96
58004.501	10.16	9.30	8.43	7.90	7.25	6.62	5.96	5.09	4.95
58008.546	...	...	...	...	7.26	6.62	5.95	5.03	4.77
58026.556	...	...	...	...	7.23	6.58	5.92	5.00	4.78
58038.401	10.49	9.55	8.64	8.07	7.35	6.66	5.96	5.00	4.79
58066.348	10.55	9.61	8.66	8.10	7.34	6.64	5.90	4.91	4.69
58096.335	10.38	9.45	8.55	8.00	7.29	6.61	5.89	4.87	4.60
58100.369	...	...	...	...	7.35	6.66	5.91	4.92	4.64
58114.373	10.60	9.64	8.69	8.13	7.36	6.65	5.90	4.84	4.54
58120.191	10.66	9.67	8.71	8.12	7.31	6.63	5.87	4.87	4.63
58125.323	11.07	10.00	8.96	8.33	7.53	6.75	5.98	4.93	4.75
58126.193	10.94	9.88	8.88	8.25	7.46	6.73	5.96	4.91	4.67
58143.030	12.03	10.82	9.64	8.86	7.84	6.94	6.06	4.93	4.57
58144.238	11.95	10.72	9.56	8.79	7.81	6.94	6.03	4.94	4.64
58151.174	10.88	9.83	8.83	8.21	7.42	6.70	5.90	4.88	4.61